Arabian Journal for Science and Engineering (2021) 46:7875–7892
https://doi.org/10.1007/s13369-021-05617-4

RESEARCH ARTICLE-MECHANICAL ENGINEERING

Mechanical Property and Prediction Model for FDM-3D Printed Polylactic Acid (PLA)

M. Samykano[1]

Received: 2 December 2020 / Accepted: 24 March 2021 / Published online: 8 April 2021

Abstract
Fused deposition modeling (FDM) has been the preferred technology in 3D printing due to its ability to build functional complex geometry parts. The lack of the printing parameter information and prediction model that directly reflects towards 3D printed part's mechanical properties has been a barrier for the FDM 3D printer users to appraise the product's strength as a whole. In the present work, 27 tensile specimens with different parameter combinations were printed using a low-cost FDM 3D printer according to the ASTM standard to evaluate their tensile properties. Statistical analysis was performed using MINITAB to validate the experimental data and model development. The investigational outcomes reveal that ultimate tensile strength was primarily affected by infill density, whereby it increases with increasing infill density. Elastic modulus, fracture strain, and toughness were mainly affected by infill density and layer thickness. The ideal printing parameter for optimal tensile behavior was identified to be 0.3 mm layer height, 40° raster angle, and 80% infill density from the 9th combination. The tensile values obtained for the optimal printing parameter were 28.45150 MPa for ultimate tensile strength, 0.08012 mm/mm for fracture strain, 828.06000 MPa for elastic modulus, 20.19923 MPa for yield strength, and 1.72182 J/m^3 for toughness. The statistical analysis further affirmed the optimum printing has a minimal deviation from the experimental response. Finally, a mathematical model is proposed for the tensile properties prediction.

Keywords Fused deposition modeling · 3D printing · RSM · Mechanical test · PLA

1 Introduction

The fast-changing customer demands, the need for high-quality products at the lowest possible cost and the elegant aesthetic effect have emerged the FDM 3D printing technology. FDM 3D printing is a well-known technique for producing tangible prototypes from various materials [1, 2]. This technology is vastly favored in today's high-speed design-to-market workplaces for its quick and inexpensive prototypes. Having the ability for direct manufacturing, producing products with complex geometry, freedom for innovative design, economical use of material, and being environmentally friendly that surpasses traditional manufacturing limitations has been the core reason for this evolution [3]. In FDM, as shown in Fig. 1, the thermoplastic filament is melted using a heating cartridge placed in the block, extruded through a nozzle with the help of a pinch feed mechanism, and deposited on the hotbed layer-by-layer up until the formation of an intended product [4]. The most common materials utilized in this technology are amorphous thermoplastics such as Acrylonitrile Butadiene Styrene (ABS) and Polylactic Acid (PLA) [5–7]. Due to their lightweight, inexpensive and formability, these thermoplastics have been highly preferred in the engineering and medical fields [8].

Since mechanical properties are essential for functional parts, it is necessary to study and understand how such properties may vary with different materials and processing parameters. Thus, improvement can be made suitably during the fabrication phase to improve its properties [9]. The printed component properties were reported to depend on the layer fusions' strength. The interface strength is the most significant as the two layers' thermal gradient determines the functional components' final properties. This fusion's strength depends on many factors such as temperature gradient, polymer structure (molecular weight, branching, heat

✉ M. Samykano
mahendran@ump.edu.my

[1] Department of Mechanical Engineering, College of Engineering, Universiti Malaysia Pahang, 26300 Gambang, Pahang, Malaysia

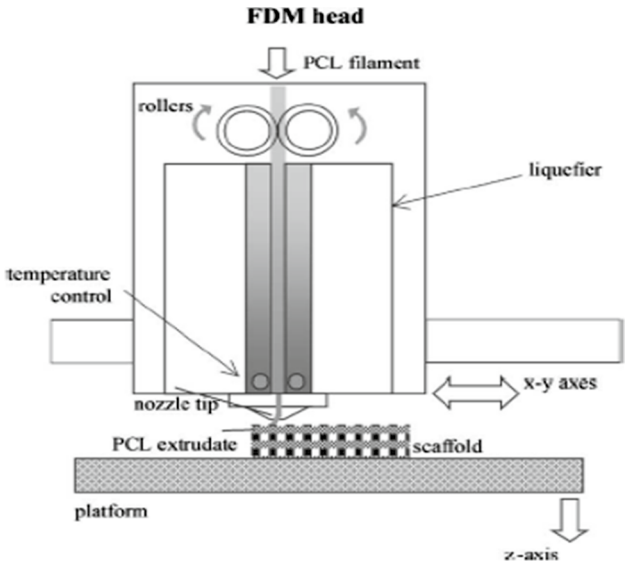

Fig. 1 A schematic diagram of the FDM extrusion and deposition process [11]

of fusion, glass transition temperature), and bead geometry [10].

Apart from the fusion strength, FDM's properties also reliant on six critical printing factors such as layer height, air gap, extrusion temperature, raster angle, printing speed, and infill percentage [12–14]. These factors are defined as follows: (1) Layer height: the Z-axis's height relative to the printing bed directly reflects the deposited layer's thickness. The layer height should not be greater than the nozzle diameter. (2) Air gap: the space between the beads. Positive gap results in a loosely packed structure that builds rapidly. Meanwhile, the negative gap allows two beads to partially occupy the same space. These results in a more dense structure, which requires a longer build time. The negative gap settings were also shown could minimize the voids. (3) Extrusion temperature: the temperature at which the filament is melted and extruded for deposition on the hotbed. (4) Raster angle: the angle or direction of the beads of material about the part's loading. The different modes and directions used will affect the part's mechanical properties. (5) Printing speed: the speed of extruder motion in the *x*- and *y*-axis during the printing process. (6) Infill percentage: The amount of deposited material on each surface layer.

As to date, quite a number of studies have been performed to investigate the effect of printing parameters on 3D printed parts' mechanical behavior. A study conducted by B.M Tymrak et al. shows that the tensile strength changes with the extruded filament alignment on the loading direction due to different build orientations [15]. The tested ABS printed specimen showed higher tensile strength at the layer height of 0.2 mm and 45° raster angle. In another study conducted by Sung-Hoon et al., the effect of raster pattern and air gap on the printed ABS specimen's tensile strength was investigated [16]. Their finding reports that at zero air gap, the specimen built at 0° has greater tensile strength than the specimen made at 90°. Also, at -0.003 air gaps, all the tested specimens showed an increase in the overall tensile strength. In another investigation, the tensile properties of polyetherimide (PEI) specimens reveal that each build direction has different tensile strength and strain characteristics. Test specimens produced in the *X*-direction were reported to have the best strength and elongation before the failure, followed by *Y*-direction and *Z*-direction [17]. Hongbin Li et al. investigated the effects of layer thickness, deposition velocity, and infill rate on PLA bonding strength. They found that layer thickness plays a predominant role in affecting the bonding strength, followed by deposition velocity and infill rate [18].

Es-Said et al. examined the effect of raster orientation on ABS's mechanical properties. They reported that raster orientation significantly influences the polymer molecules [19]. Habbeb et al. conducted a study on the relationship between PLA material's strength and porosity in FDM 3D printing through standard tensile tests. Their findings show that the printed parts' highest average tensile strength was 45.56 MPa at 0.2 mm layer height for PLA. The porosity of PLA was found to be increasing with layer height [20]. Xunfei Zhou et al. evaluated the printing pattern and infill density effects on the ultimate tensile strength and elastic modulus. Their experimental results revealed minimizing air gaps and using a triangular infill pattern consequences good UTS [21].

Apart from the experimental investigation, the mathematical model development has also gained importance in estimating the mechanical properties of parts produced via an FDM 3D printer. However, it is still limited compared to the number of experimental investigations. Pires et al. [22] developed a prediction model to explore the critical printing factors such as mass, mass variation, printing time, and porosity on the printed specimen properties. They realized that the size scale, printlet format, and print temperature influence the printlet mass, while the printing time was impacted by size scale, printing speed, and layer height. Meanwhile, Anitha et al. used Taguchi and ANOVA analysis to investigate the relationship of parts' layer thickness, road width, and deposition speed with the surface roughness and conclude that the significant factor is layer thickness [23]. Ang et al., from their analysis using full factorial design, proved that all input parameters consist of an air gap, raster width, build orientation, build laydown pattern and build layer are significant to the response, which is porosity, compressive strength, and compressive modulus [24, 25]. Thus, the present work investigates the PLA's tensile behavior using the FDM 3D printing technique [7] and proposes a mathematical model to predict those properties.

2 Materials and Methods

Rainstorm Desktop 3D Multicolor Printing Printer Reprap Prusa i3 with a 0.4 mm nozzle diameter was used to fabricate the tensile test specimen using a 1.75-mm PLA filament. Arduino Mega 2560 was used as the microcontroller and RAMPS 1.4 attached to the Arduino Mega 2560 to expand pin inputs. The Marlin firmware open-source software and the Repetier Host slicing software were used to generate G-code files and control the FDM 3D printer to fabricate the desired parts. The tensile test was performed using INSTRON 3367 machine. The maximum load which can be applied to this machine is 50kN. According to the ASTM D638 standard, the suggested speed of testing is 5 mm/min. The test was conducted at the Materials Laboratory of Universiti Malaysia Pahang. Table 1 lists the parameters which have been kept constant during the printing process.

2.1 Part Fabrication Using FDM 3D Printer

The specimen design is created using a CAD program (SolidWorks 2017 edition) and saved into an (STL) file format. The STL file stores every surface of the 3D design and shows it as triangulated segments. The FDM 3D printer reads the digitally supplied coordinates resultant from the STL file by transforming it into a G-file via slicer software present in the FDM 3D printer. The G-code file divides the 3D STL file into a sequence of two-dimensional (2D) horizontal cross-sections (25–100 µm) depending on the fabrication technique [26]. During fabrication, the thermoplastic polymer's filament is fed into an extruder containing a heater to liquefy the filament. The filament is dragged inward with a pinch feed mechanism's help and extrudes the molten bead of material through a circular nozzle. The moveable FDM head then deposits the extruded material layer-by-layer onto the substrate. The melting of the material performed 1 degree above its melting point, allowing it to solidify immediately upon deposition [27]. These allow for good bondage between the layers. The extruder head moves according to the layer height and repeats the layer deposition cycle until the original CAD file's full physical representation is formed [28]. Figure 2a shows the printed specimen used for the mechanical tests, while Fig. 2b depicts the geometry of the Type 1 specimen according to the ASTM D638 standard. Table 2 lists the dimension of the Type 1 specimen adapted according to the ASTM D638 standard.

2.2 Design and Realization of the Experiment

The experiment design starts with parameter selection, the type of test to be conducted, and the number of specimens required for the analysis. A total combination of 3 values from 3 types of the parameter was chosen. Three chosen parameters for the investigation are layer height, raster angle, and infill density. Infill density is the amount of material (in percentage) used to print the part. The higher the infill

Table 1 Printing parameters and their values

S. no.	Parameters	Values (constant)
1	First layer height	0.3 mm
2	Horizontal Shell: a solid layer	Top and Bottom 3 layers
3	Fill pattern	Line
4	Printing speed	30 mm/s
5	Nozzle diameter	0.3 mm
6	Filament diameter	1.75 mm
7	Extruder temperature	195 °C
8	Print bed temperature	110 °C

Table 2 Dimensions of the Type 1 specimen geometry according to ASTM D638 standard

Dimensions	Values (mm)
W	13
L	57
WO	19
LO	165
G	50
D	115
R	244
T	3.2

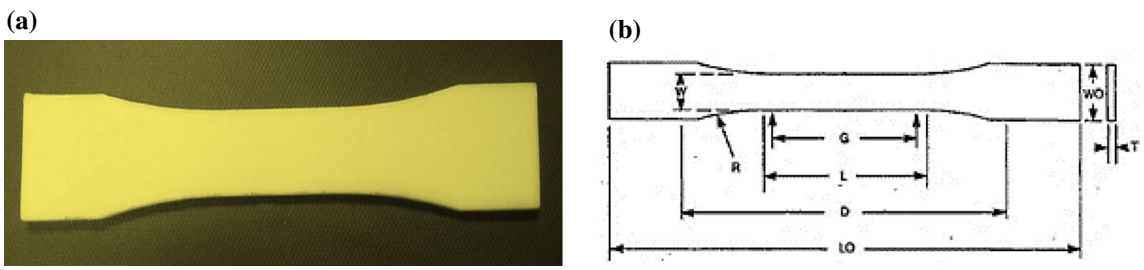

Fig. 2 **a** PLA printed tensile specimen, **b** Type 1 specimen geometry according to ASTM D638 standard

percentage, the higher the amount of material used to print the part. The infill density chosen for the present investigation is 20, 50, and 80%. The layer height is the thickness of each layer of material deposition during the printing process. The chosen layer height for the present work is 0.1, 0.2, and 0.3 mm. Raster angle is the angle of material deposition referencing the printing axis. The chosen value for the raster angle is 40, 60 and 80°. The mechanical test to be undertaken is a tensile test. The samples were printed and tested according to the ASTM D638 Type 1 standard [29]. All the parameters are set in slicing software before converted into a G-code file. Using DOE, the total amount of combination for all three parameter value variations is obtained to be 27 sets of data, as shown in Table 3. 27 different combined parameters were printed to study how differently each combination affects the PLA specimen's mechanical properties. Three samples were prepared for each set of data required and averaged. In total, 81 specimens were printed for the experimental analysis. The tensile testing was performed to assess the tensile property of each sample upon completion of the printing. The finding was analyzed in the form of the tabulation of ultimate tensile strength, fracture strain, and elastic modulus. The generated graph was studied, and the necessary information was extracted.

2.3 Design of Experiment Analysis Using Response Surface Methodology (RSM)

Statistical analysis was done using the obtained experimental data for validation purposes to support this experiment's reliability. The analysis was completed using a full factorial approach using MINITAB software. This statistical evaluation aims to evaluate the effect of three combined printing parameters: infill layer height, raster angle, and infill density towards the tensile properties of the FDM 3D printed PLA and the development of a mathematical model for tensile properties prediction. From the statistical evaluation, an ANOVA of variance table was generated to depict the

Table 3 The list of ultimate tensile strength, fracture strain, elastic modulus yield strength, and energy absorption of each specimen

No.	Layer height (mm)	Raster angle (°)	Infill density (%)	Ultimate tensile strength (MPa)	Fracture strain (mm/mm)	Elastic modulus (MPa)	Yield strength (MPa)	Energy absorption (J/m^3)
1	0.1	40	20	19.13284	0.04696	471.36800	14.80733	0.50202
2	0.2	40	20	20.62756	0.04749	592.43518	20.24389	0.59183
3	0.3	40	20	25.47271	0.05649	664.50571	23.25575	0.81519
4	0.1	40	50	20.01269	0.04944	617.45320	18.20973	0.50670
5	0.2	40	50	22.07215	0.05638	681.82740	25.96373	0.58856
6	0.3	40	50	27.60767	0.06299	687.48530	25.41023	0.96247
7	0.1	40	80	32.93754	0.05201	807.48931	26.08234	0.89816
8	0.2	40	80	25.98610	0.06221	811.80500	17.15938	1.04959
9	0.3	40	80	28.45150	0.08012	828.06000	20.19923	1.72182
10	0.1	60	20	9.737220	0.03667	277.74950	9.02682	0.18207
11	0.2	60	20	14.62170	0.04234	411.37350	11.71857	0.33722
12	0.3	60	20	21.89921	0.04725	569.91250	17.94593	0.57895
13	0.1	60	50	18.62290	0.04301	502.59040	15.39083	0.42085
14	0.2	60	50	23.50263	0.05779	548.66390	17.06961	0.80591
15	0.3	60	50	29.91145	0.05955	666.89560	22.90661	0.99215
16	0.1	60	80	27.74211	0.04633	688.12960	22.57436	0.67791
17	0.2	60	80	34.44592	0.05962	765.41520	12.13855	1.18200
18	0.3	60	80	31.31328	0.07797	779.47400	15.59510	1.82228
19	0.1	80	20	17.45173	0.04544	441.46120	15.45240	0.43158
20	0.2	80	20	24.13670	0.04641	545.66240	21.76234	0.57730
21	0.3	80	20	21.26233	0.05212	620.03750	16.53470	0.65563
22	0.1	80	50	21.33669	0.04587	563.48140	17.40802	0.55962
23	0.2	80	50	26.51747	0.04700	637.79120	22.64616	0.66814
24	0.3	80	50	24.16019	0.05428	671.07330	20.64242	0.76498
25	0.1	80	80	35.61776	0.04823	912.16466	19.77362	0.94174
26	0.2	80	80	31.40398	0.05116	930.57890	17.84010	0.96893
27	0.3	80	80	32.13470	0.05637	952.17360	18.04070	1.08333

p-value of the involved factors. The confidence level for the analysis was set to be 95%; thus, any *p*-value higher than 0.05 is considered an insignificant effect on the resulting tensile property. The generated regression equation reliability was determined by calculating the error percentage between the experimental and predicted value. If the average error percentage is below 10%, then the model is considered reliable. Finally, a response optimizer is used to determine the maximum individual and overall mechanical response with regard to printing parameter combination.

3 Results and Discussion

Five different groups of graphs denoting specific tensile behavior have been plotted according to each printing parameter. The plot is generated to visualize any observable trend that could be concluded related to the effect of selected parameter combinations on tensile properties.

As shown in Table 3, the tensile properties, which are the ultimate tensile strength, elastic modulus, yield strength (0.2% offset), fracture strain, and energy absorption, are deduced from stress–strain curves individually. The overall stress–strain curve of all the specimens is shown in Fig. 3. Meanwhile, Figs. 4 and 5 depict the fractured images captured using a light microscope.

3.1 Ultimate Tensile Strength (UTS): Effect of Infill Percentage, Raster Angle, and Layer Thickness

The ultimate tensile strength (UTS) is the material's maximum resistance to fracture. It is equal to the maximum load that can be carried by one square inch of the cross-sectional area when the load is applied in tension. The UTS

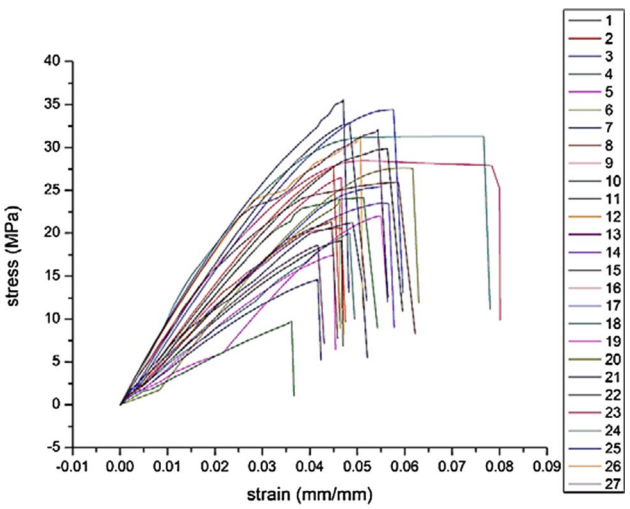

Fig. 3 Stress versus strain curves for all 27 combinations

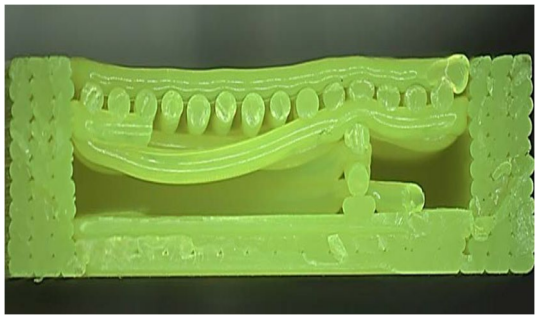

Fig. 4 Polymer chains across the interface

can differ depending on the type of material. The UTS is usually obtained by performing a tensile test and plotting the engineering stress versus strain curve. The highest point of the stress–strain curve is UTS. It is an intensive property; therefore, its value does not depend on the test specimen's size. However, it is dependent on other factors, such as preparation parameters, the presence of surface defects, the temperature of the test environment, and the material.

In this project's context, the plot reflects the average from findings for all 81 FDM 3D printed PLA specimens. Figure 6 shows that the UTS values fall between 9.737220 and 35.61776 MPa, which denotes the highest and lowest of all recorded values. The maximum tensile strength was achieved by specimen printed at 25th combination, where else the lowest was specimens printed at the 10th combination. The graphs above show the relationship between the UTS and infill percentage, raster angle, and layer thickness. It can be observed that specimens printed with 80% infill percentage resulted in higher UTS than the lower infill percentage specimen. The trend shows that when the infill density increases, the UTS also increases. Higher infill implies higher material availability to overcome the applied stress internally. From the UTS versus layer thickness graph, a strong relationship could not be construed. However, the 25th combination with 0.1 mm layer height recorded the highest UTS. The resultant increase may due to the increase in the diffusion between adjacent layers. The present findings

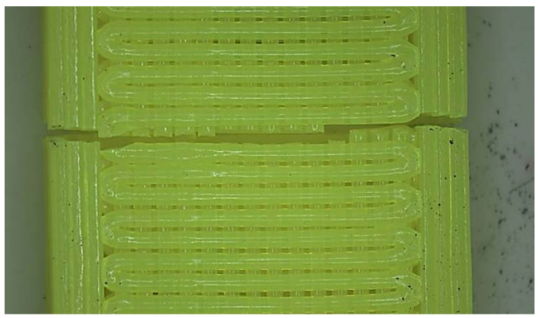

Fig. 5 Brittle fracture of PLA specimen

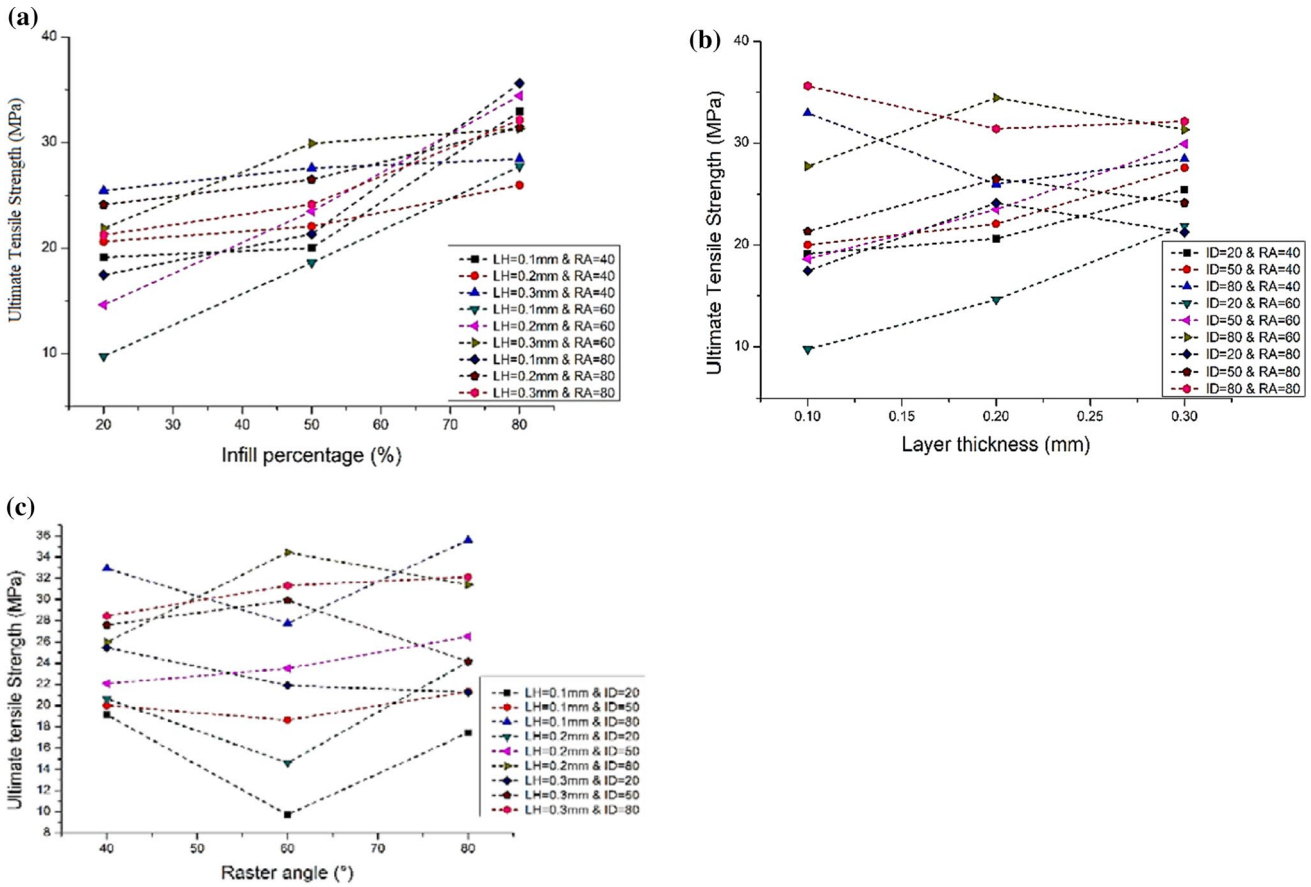

Fig. 6 **a** Ultimate tensile strength versus infill density; **b** Ultimate tensile strength versus layer thickness; **c** Ultimate tensile strength versus raster angle plot. *Note*: *ID* infill density, *LH* layer thickness, *RA* raster angle

are in favor of the previous research finding reported by BM. Tymrak, whereby he found tensile strength to be highest at lowest layer height. Meanwhile, the high-temperature gradient that increases the distortion effect, which accumulates the residual stresses, might be why the reduced UTS for a few specimens. From the UTS versus raster angle graph, there was also no apparent trend observed. However, a high raster angle is preferred due to the raster's inclination along the loading direction, offering more resistance for strength improvement [30].

3.2 Fracture Strain: Effect of Infill Percentage, Raster Angle, and Layer Thickness

Fracture strain is the maximum strain value achieved by a specimen before it fractures. It denotes the ratio between changed length and initial length after breakage of the test specimen. The fracture strain is influenced by several factors, such as strain speed, temperature, specimen geometry, and material type. The stress–strain curve for brittle materials is typically linear over their full range of strain, eventually terminating in fracture without appreciable plastic flow.

In the present study, the range of fracture strain achieved is from 0.03667 to 0.08012 mm/mm, which denotes the highest and lowest fracture strain recorded among all parameter combinations. As seen in Fig. 7, the highest fracture strain is achieved by specimens printed with the 9th combination, and the lowest is from specimens printed at the 10th combination. Upon observation from the plot, it is found that the higher infill percentage contributes to the higher fracture strain for all samples. Noticeably, the 9th combination printed with 80% infill has the highest fracture strain, while the 10th combination has the lowest fracture strain printed at 20% infill density. Generally, the higher infill specimen is more robust due to their higher degree of resistance [7]. When the specimen is more robust, the amount of strain needed to fracture the specimen is higher. Meanwhile, the raster angle shows no significant trend with respect to the resulting fracture strain. High raster angle increases the stress accumulation along the deposition's direction, resulting in more distortion and weak bonding. The fracture strain

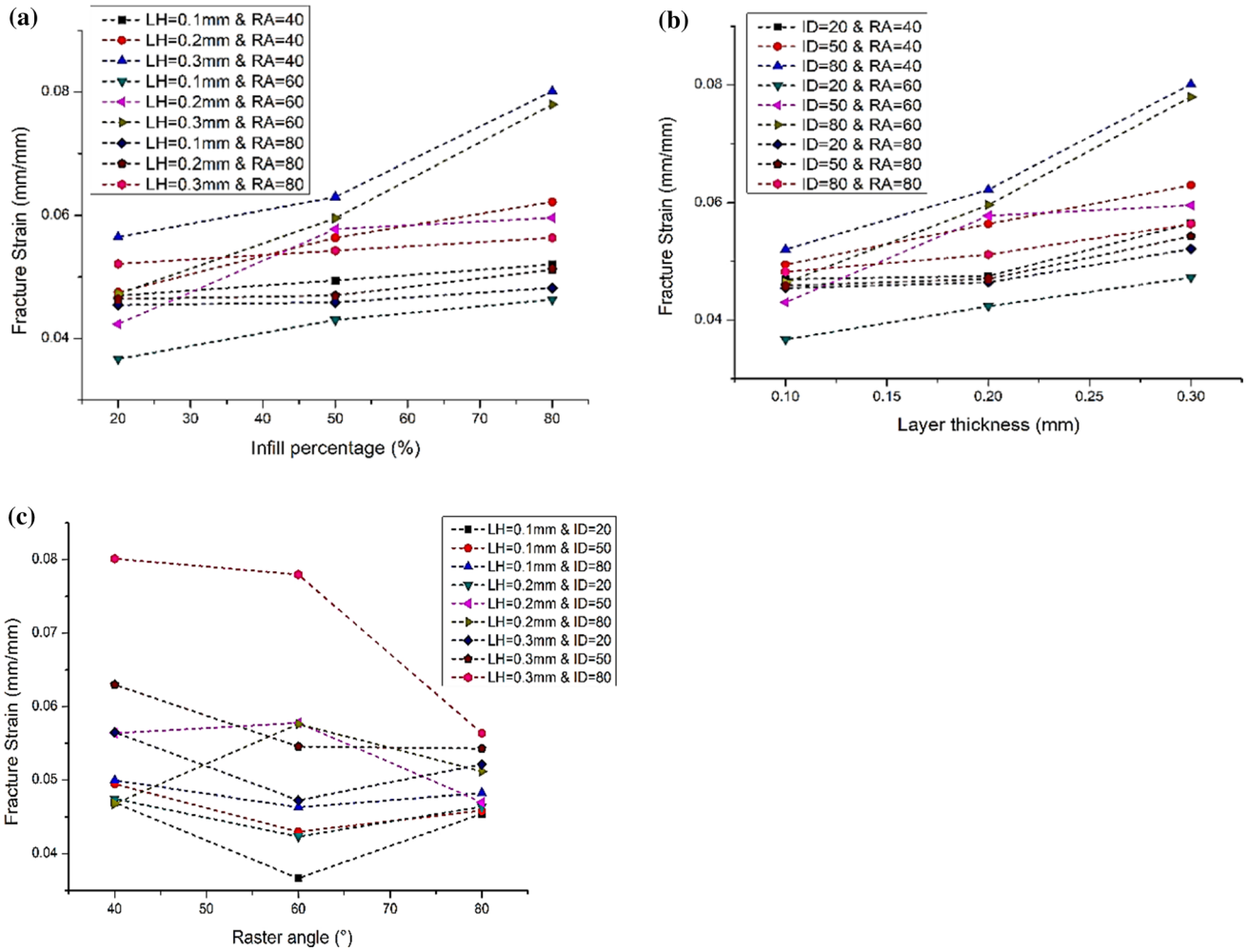

Fig. 7 **a** Fracture strain versus infill chart; **b** Fracture strain versus layer thickness; **c** Fracture strain versus raster angle plot. *Note*: *ID* infill density, *LH* layer thickness, *RA* raster angle

versus layer thickness chart displays increased fracture strain with increased layer height. This can be related to a lower distortion effect resulting from a lower temperature gradient at the bottom layer due to the higher layer height. Specimen printed with 10th combination results in the lowermost fracture strain due to the lowest infill percentage, higher raster angle, and lowest layer height.

3.3 Elastic Modulus: Effect of Infill Percentage, Raster Angle, and Layer Thickness

An elastic modulus, or modulus of elasticity, is a number that measures an object or substance's resistance to being deformed elastically when a force is applied. The elastic modulus is defined as the slope from the stress–strain curve in the elastic deformation region. It is also defined as a constant of proportionality, which varies for different materials. It is a measure of the stiffness of a given material. A stiffer material will have a higher elastic modulus. If the slope is steep, the sample is anticipated to have a high tensile modulus. If the slope is gentle, then the sample is predicted to have a low tensile modulus.

As shown in Fig. 8, the range of elastic modulus values obtained in the present study falls between 952.1736 and 277.74950 MPa, whereby it denotes the highest and lowest elastic modulus value. The highest elastic modulus is achieved by specimens printed at the 27th combination, and the lowest was the 10th combination. From the graph, it can be noticeably seen that when the infill percentage increased, the resulting elastic modulus increases. On a side note, the elastic modulus is always directly proportional to the UTS. The 27th combination printed using 80% infill is seen to have the most significant elastic modulus, while the 10th combination printed with 20% infill has the lowest elastic modulus. It also observed that when the layer height increases from 0.1 to 0.3 mm, the elastic modulus

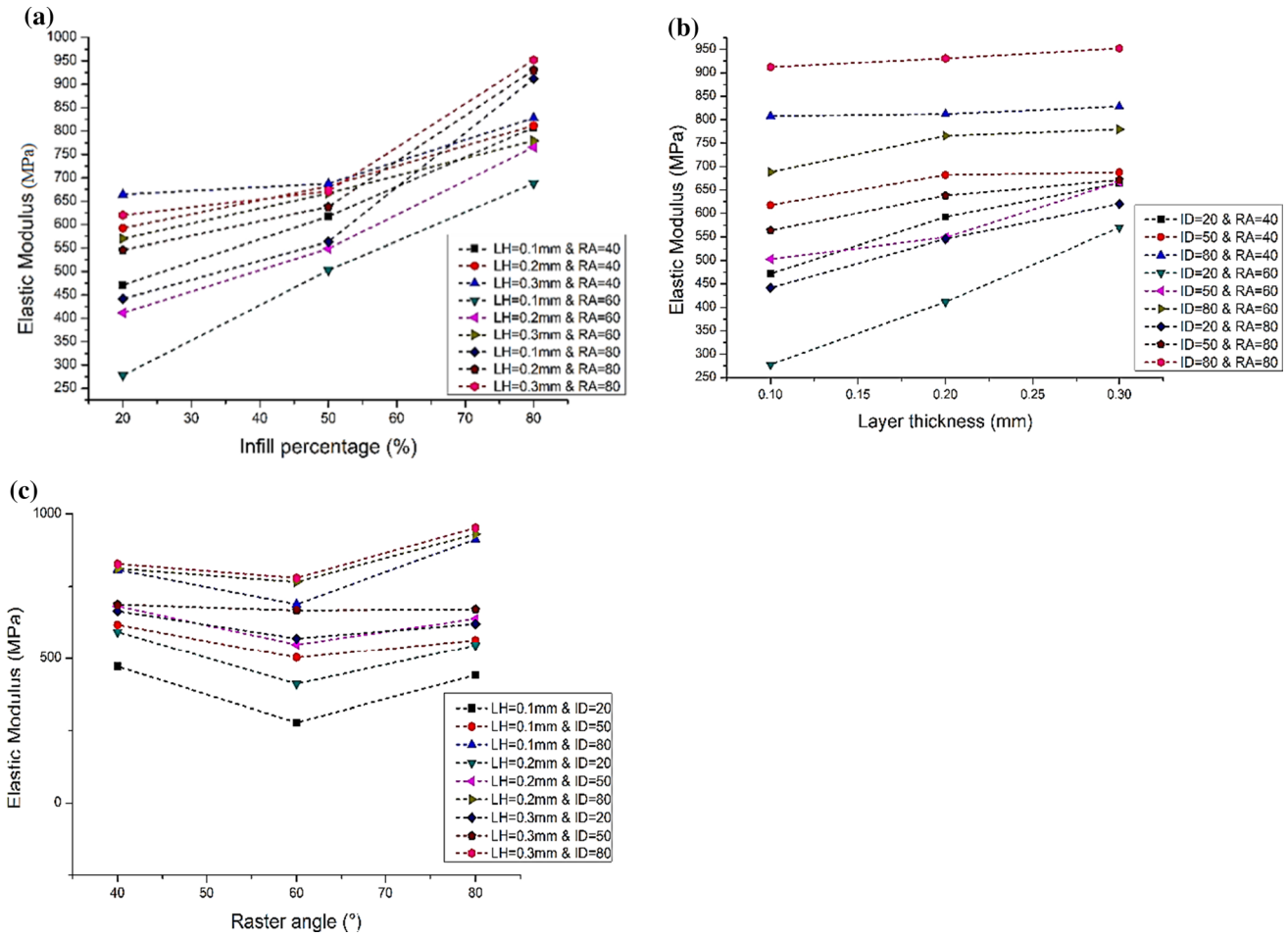

Fig. 8 **a** Elastic modulus versus infill chart; **b** Elastic modulus versus layer thickness; **c** Elastic modulus versus raster angle plot. *Note*: *ID* infill density, *LH* layer thickness, *RA* raster angle

correspondingly increases. Besides that, both 40° and 80° raster angles resulted in averagely the identical elastic modulus. The lower inclination raster angle opposite the loading direction reduces the degree of resistance, affecting their overall strength and vice versa. The maximum value of the elastic modulus is reached when all fibers are oriented along the loading line. In this condition, the specimen shows the highest stiffness as each fiber takes the load, and the effects of the fiber-to-fiber bonding are minimized. Infill orientation close to 0° reduces strength and stiffness because the bonding surfaces take part in the tensile load among fibers, weaker, and more prone to fail [1].

3.4 Yield Strength (0.2% Offset): Effect of Infill Percentage, Raster Angle, and Layer Thickness

Yield strength is defined as the yield stress, which is the stress level at which permanent deformation of 0.2% of the material's original dimension occurs. It is also defined as the stress level at which a material can withstand before it deformed permanently. Before reaching the yield point, the material will distort elastically and return to its original shape upon removing repression and stress. Beyond the yield point, the deformation will be permanent and cannot be reversed. There will be little or no plastic deformation in brittle materials, and fracture occurs around the end portion of the linear elastic curve.

From Fig. 9, the highest yield strength achieved is 26.08234 MPa and ranges down to 9.02682 MPa. The 7th combination records the maximum yield strength, and the 10th combination records the lowest. Specimens with the 7th combination printed with 80% infill again result in the highest yield strength. However, there are several specimens that shown an opposite trend, whereby the smaller infill percentage has resulted in higher yield strength. From the graph, it can be inferred that infill density has a varied effect on yield strength. A uniform trend can only be noticed for the infill density from 20 to 50%. The yield strength increases with the increase in infill density. From the yield strength versus raster angle graph, the lowest raster angle, which is

40° resulted in considerably high yield strength compared to higher raster angle. The intermediate raster angle has mostly been seen to cause a significant drop in yield strength. While evaluating the effect of layer height on the yield strengths, it can be concluded that there is no legit trend. The impact of layer height is disseminated with respect to the printing parameter combination. The 10th combination recorded the lowest value of ultimate strength, fracture strain, elastic modulus, and yield strength on a side note.

3.5 Toughness (Energy Absorption)

Toughness is defined as a material's ability to deform plastically and absorb energy in the process before fracturing. In other words, resistance to fracture. Toughness is directly proportional to the combination of strength and ductility. For instance, a material with high strength and ductility will be tougher than a material with low strength and high ductility. Strength refers to the ability to resist deformation upon the placement of stress. Ductility is the strain experienced before fracture, whereby the percentage of elongation is the indicator in a uniaxial tensile test. Calculation of area under the stress–strain curve is one way to measure the toughness. The calculated area value is denoted as "material toughness," and it has units of energy per volume (J/m^3).

Figure 10 shows the highest toughness achieved is 1.82228 J/m^3 and ranges down to 0.18207 J/m^3. The maximum toughness is recorded by the 18th combination, while the lowest is from the 10th combination. Specimens with 18th combination are printed with 80% infill, 60° raster angle, and 0.3 mm layer thickness. Toughness shows an increasing trend with infill percentage and layer thickness. Raster angle shows a varied effect with all the parameter combinations, whereby in some cases, 40° raster angle resulted in higher toughness compared to other raster angles and vice versa.

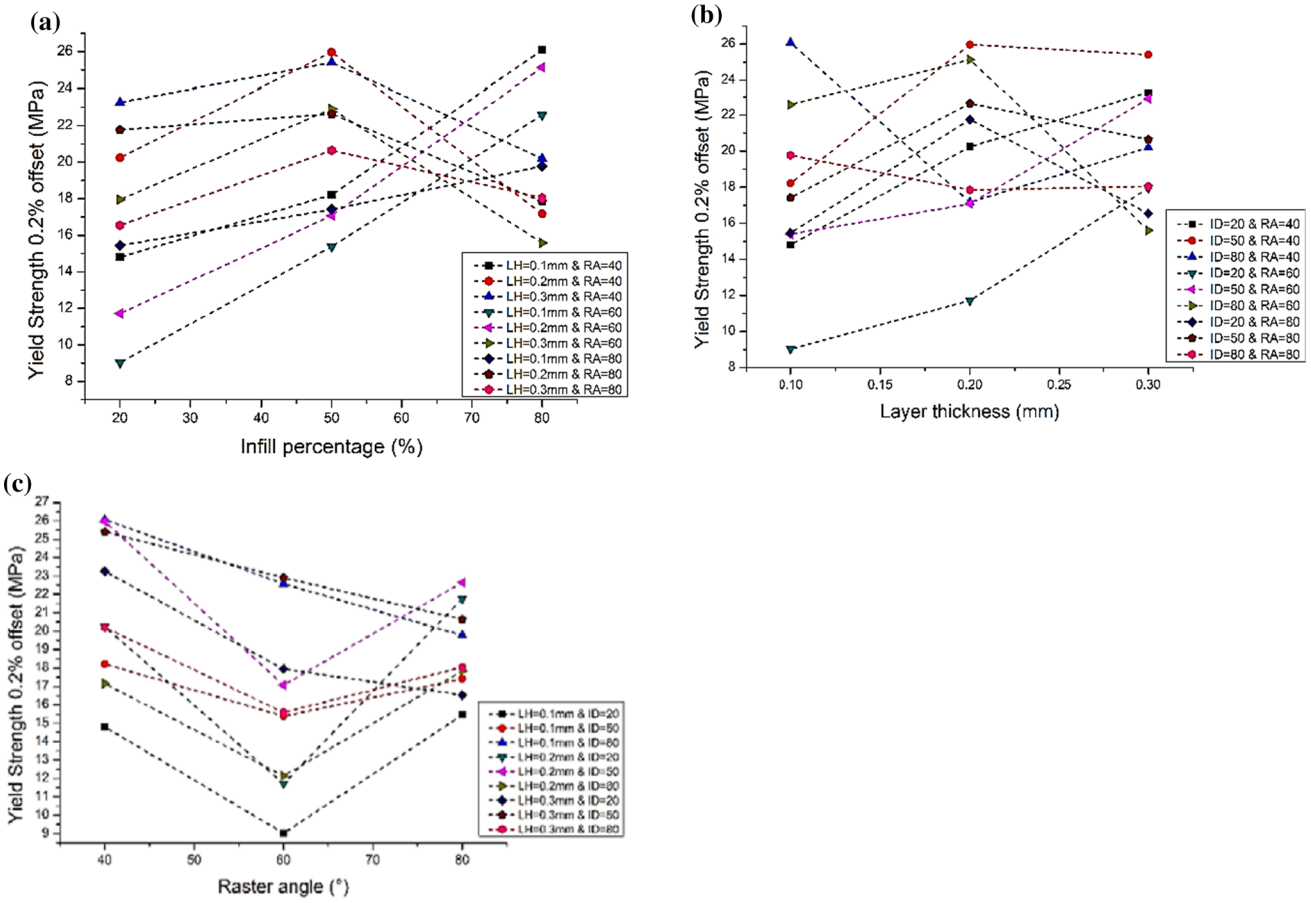

Fig. 9 **a** Yield strength versus infill chart; **b** Yield strength versus layer thickness; **c** Yield strength versus raster angle plot. *Note*: *ID* infill density, *LH* layer thickness, *RA* raster angle

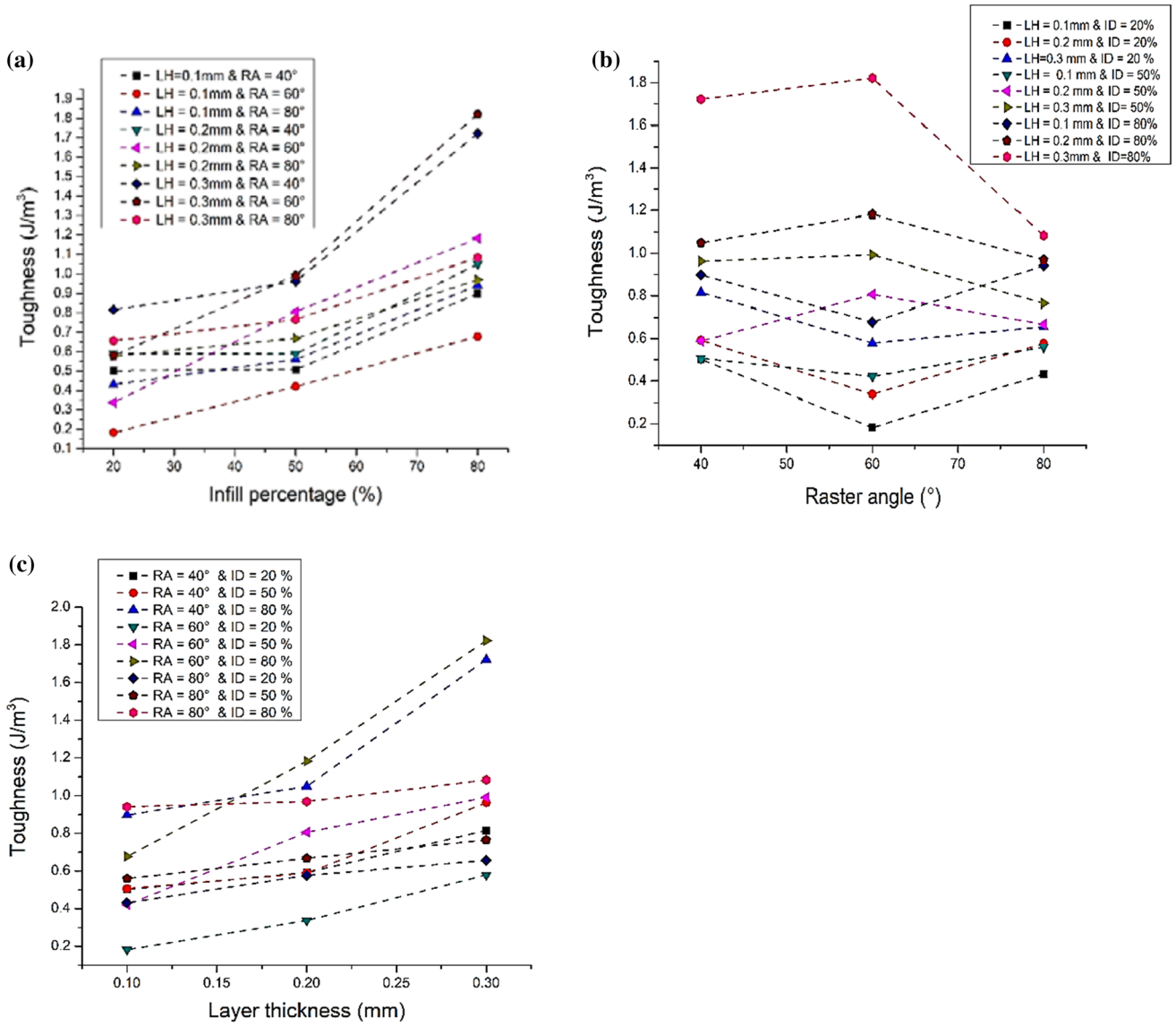

Fig. 10 **a** Toughness versus infill density; **b** Toughness versus raster angle; **c** Toughness versus layer thickness plot. *Note*: *ID* infill density, *LH* layer thickness, *RA* raster angle

4 Design of Experiment Analysis using Response Surface Methodology (RSM)

4.1 Ultimate Tensile Strength (UTS)

Table 4 shows that the *p*-value of layer height and infill percentage is lesser than the alpha value, which is 0.05, indicating its significant effect on the ultimate tensile strength. The infill density is the most significant parameter influencing the UTS and is followed by layer thickness. The 2-way interaction is insignificant since its *p*-value is more than 0.05. Other combinations of the parameters are also seen to be inconsequential since the *p*-value more than 0.05. The R^2 is more than 80% suggesting reliable experimental data. The developed second-order mathematical model is shown in Eq. 1. The contour plot shown in Fig. 11 suggests the maximum UTS can be obtained with a higher layer height and high raster angle.

Table 4 ANOVA table for UTS

Source	DF	*F*-Value	*p*-Value
Model	9	8.38	0.000
Linear	3	21.72	0.000
Layer height (mm)	1	7.94	0.012
Raster angle (°)	1	0.70	0.416
Infill density (%)	1	56.53	0.000
Square	3	1.01	0.412
Layer height (mm) * Layer height (mm)	1	0.01	0.941
Raster angle (°) * Raster angle (°)	1	1.81	0.197
Infill density (%) * Infill density (%)	1	1.22	0.285
2-Way interaction	3	2.41	0.102
Layer height (mm) * Raster angle (°)	1	0.30	0.590
Layer height (mm) * Infill density (%)	1	5.42	0.033
Raster angle (°) * Infill density (%)	1	1.52	0.234
Error	17		
Total	26		
$R^2 = 81.61\%$			

Response optimizer was used to optimize the predicted ultimate tensile strength value within the range inserted printing parameter combination. From this analysis, the maximum ultimate tensile strength was found to be 34.07 MPa at a printing combination of 0.1 mm layer height, 80° raster angle, and 80% infill density.

5 Elastic Modulus

Table 5 shows that the *p*-value of layer height and infill percentage is lesser than the alpha value of 0.05, indicating its significant effect on the ultimate tensile strength. The infill density (F-value 364.83) most significantly affects elastic modulus and is followed by layer thickness. The combination of the layer height (mm) * infill density (%) and raster angle (°) * Infill density (%) was found to be significant for 2-way interaction as the *p*-value is less than 0.05. For the square, it is substantial for the raster angle (°) * raster angle (°), and infill density (%) * infill density (%). These findings

$$\begin{aligned}\text{Ultimate tensile strength (MPa)} = {} & 21.9 + 78.9\ \text{Layer height (mm)} \\ & - 0.559\ \text{Raster angle (°)} + 6.0\ \text{Infill density (\%)} \\ & - 10\ \text{Layer height (mm)} * \text{Layer height (mm)} \\ & + 0.00455\ \text{Raster angle (°)} * \text{Raster angle (°)} \\ & + 16.6\ \text{Infill density (\%)} * \text{Infill density (\%)} \\ & - 0.262\ \text{Layer height (mm)} * \text{Raster angle (°)} \\ & - 74.2\ \text{Layer height (mm)} * \text{Infill density (\%)} \\ & + 0.197\ \text{Raster angle (°)} * \text{Infill density (\%)}\end{aligned} \tag{1}$$

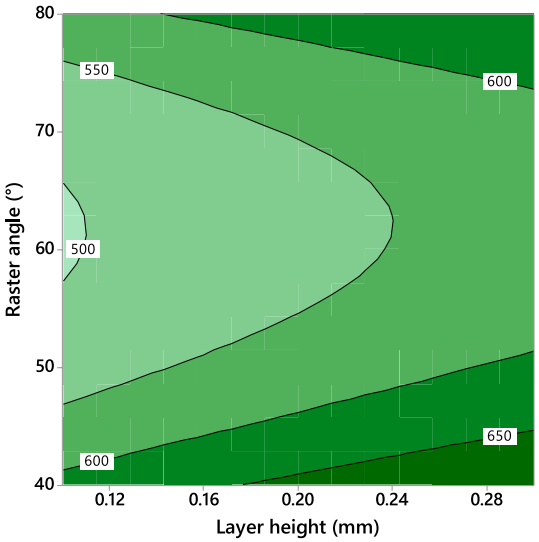

Fig. 11 Contour plot of UTS

Table 5 ANOVA table for elastic modulus

Source	DF	*F*-Value	*p*-Value
Model	9	58.70	0.000
Linear	3	141.44	0.000
Layer height (mm)	1	58.92	0.000
Raster angle (°)	1	0.55	0.468
Infill density (%)	1	364.83	0.000
Square	3	24.04	0.000
Layer height (mm) * Layer height (mm)	1	0.25	0.626
Raster angle (°) * Raster angle (°)	1	59.58	0.000
Infill density (%) * Infill density (%)	1	12.28	0.003
2-Way Interaction	3	10.63	0.000
Layer height (mm) * Raster angle (°)	1	0.12	0.735
Layer height (mm) * Infill density (%)	1	17.28	0.001
Raster angle (°) * Infill density (%)	1	14.49	0.001
Error	17		
Total	26		
$R^2 = 96.88\%$			

show that doubling the value of infill density and raster angle will affect the elastic module. The R^2 is more than 90% suggesting reliable experimental data. The developed second-order mathematical model is shown in Eq. 2. The interaction plots can be seen in Fig. 12. This graph demonstrates that the parameters interact with each other in few points. The contour plot is shown in Fig. 13.

$$\begin{aligned}\text{Elastic modulus (MPa)} = {} & 1331 + 1536\ \text{Layer height (mm)} - 36.90\ \text{Raster angle (°)} \\ & - 138\ \text{Infill density (\%)} - 720\ \text{Layer height (mm)} * \text{Layer height (mm)} \\ & + 0.2801\ \text{Raster angle (°)} * \text{Raster angle (°)} + 565\ \text{Infill density (\%)} \\ & * \text{Infill density (\%)} + 1.77\ \text{Layer height (mm)} * \text{Raster angle (°)} \\ & - 1422\ \text{Layer height (mm)} * \text{Infill density (\%)} + 6.51\ \text{Raster angle (°)} * \text{Infill density (\%)}\end{aligned} \tag{2}$$

Response optimizer was used to optimize the predicted elastic modulus value within the range inserted printing parameter combination. From this analysis, the maximum elastic modulus was found to be 936 MPa at a printing combination of 0.3 mm layer height, 80° raster angle, and 80% infill density.

6 Fracture Strain

Table 6 shows that the *p*-value of layer height and infill percentage is lesser than the alpha value of 0.05, indicating the significant effect on the ultimate tensile strength. The layer height (F-value 37.44) most significantly affects the fracture strain and is followed by infill density and raster angle. The combination of the layer height (mm) * infill density (%) was found to be substantial for the 2-way interaction since its *p*-value is less than 0.05. The findings also indicate that the increase of infill density and layer thickness for the square is insignificant. The R^2 is more than 85% suggesting reliable experimental data. The developed second-order mathematical model is shown in Eq. 2. The interaction plots

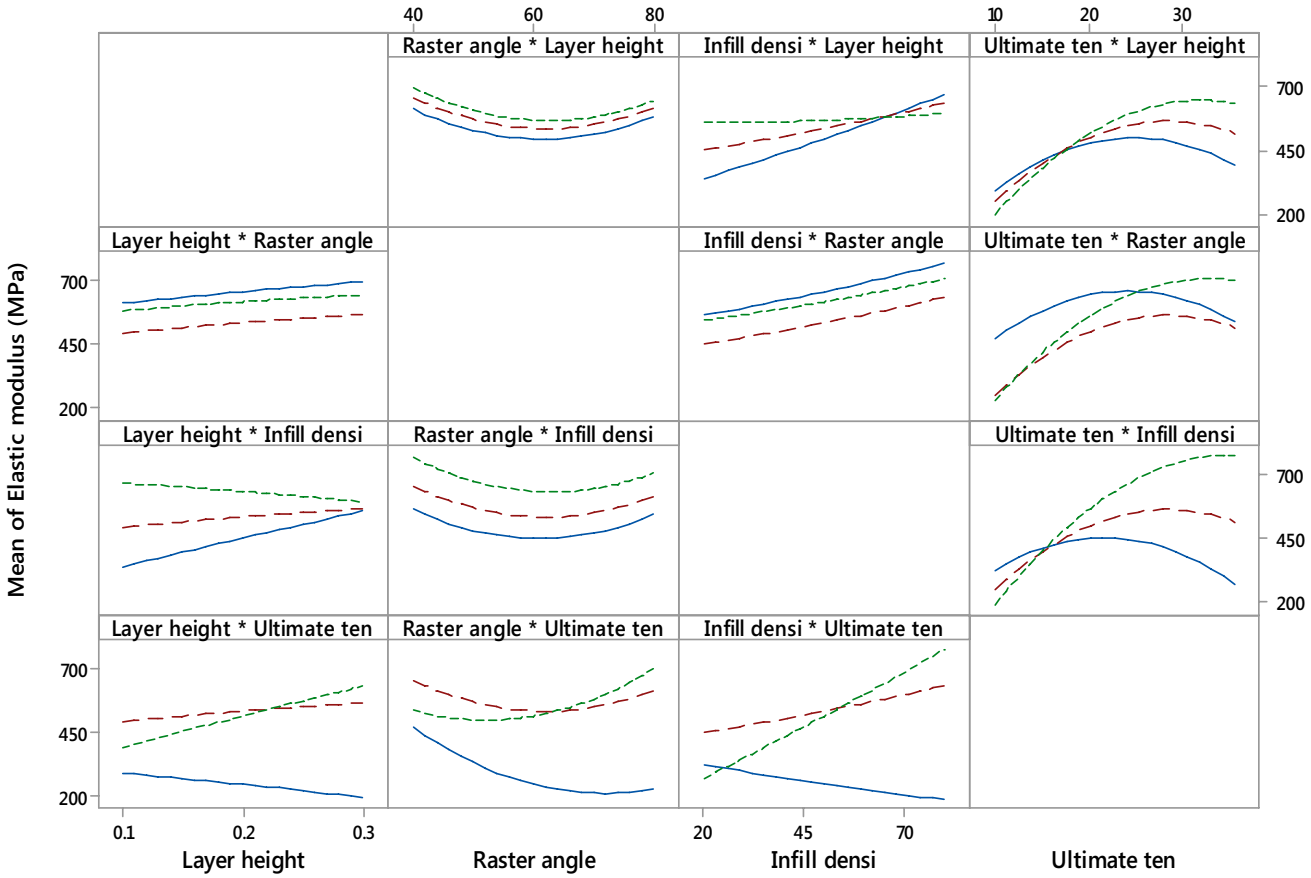

Fig. 12 2-Way interaction plot

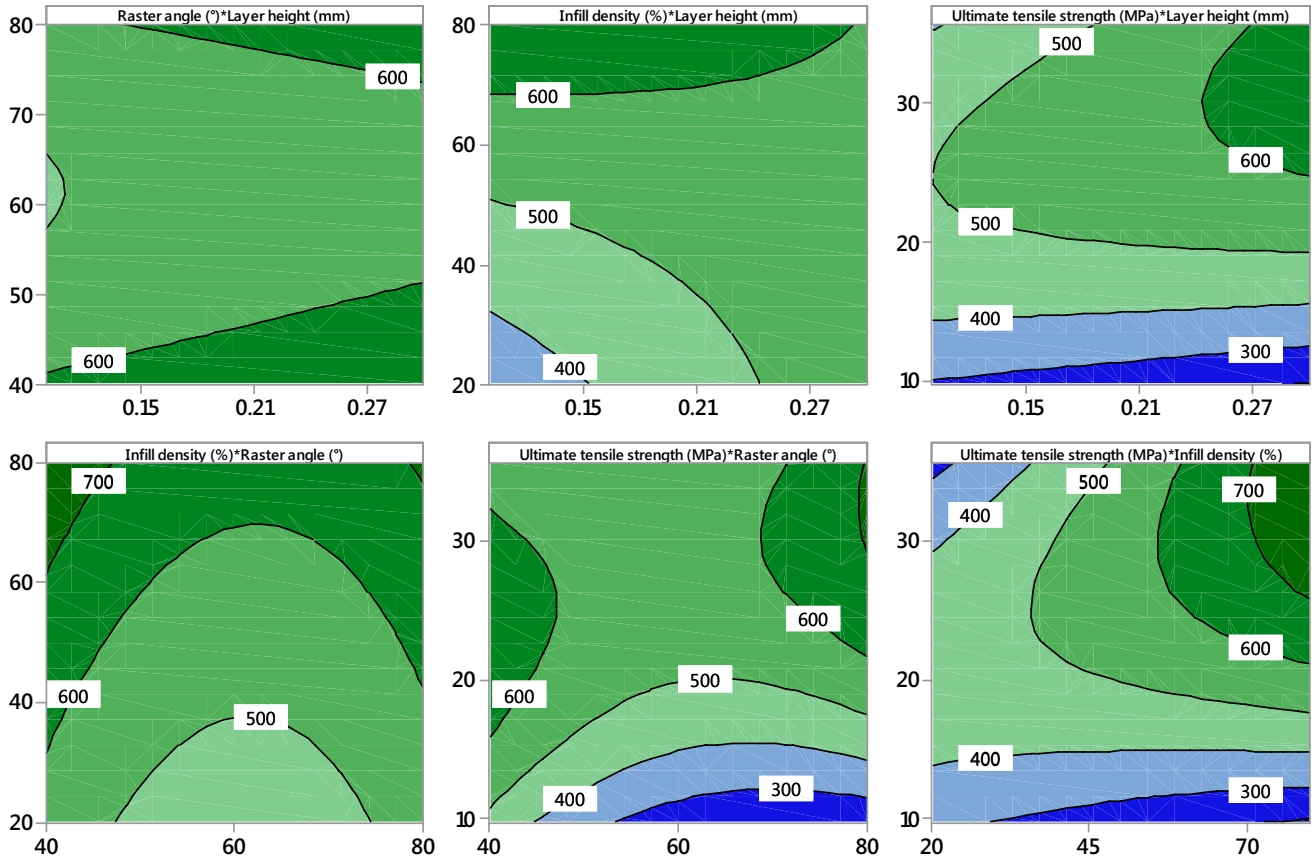

Fig. 13 The contour plot of elastic module

Table 6 ANOVA table for fracture strain

Source	DF	*F*-Value	*p*-Value
Model	9	14.43	0.000
Linear	3	37.44	0.000
Layer height (mm)	1	56.93	0.000
Raster angle (°)	1	14.50	0.001
Infill density (%)	1	40.88	0.000
Square	3	0.29	0.832
Layer height (mm) * Layer height (mm)	1	0.44	0.516
Raster angle (°) * Raster angle (°)	1	0.42	0.524
Infill density (%) * Infill density (%)	1	0.01	0.934
2-Way Interaction	3	5.57	0.008
Layer height (mm) * Raster angle (°)	1	3.76	0.069
Layer height (mm) *Infill density (%)	1	8.13	0.011
Raster angle (°) * Infill density (%)	1	4.81	0.042
Error	17		
Total	26		
$R^2 = 88.43\%$			

can be seen in Fig. 14. The graph shows that the parameters interact with each other in few points. The contour plot is shown in Fig. 15.

$$\begin{aligned}\text{Fracture strain (mm/mm)} &= 0.0365 + 0.0417\ \text{Layer height (mm)} \\ &\quad - 0.000066\ \text{Raster angle (°)} \\ &\quad + 0.0228\ \text{Infill density (\%)} \\ &\quad + 0.113\ \text{Layer height (mm)} * \text{Layer height (mm)} \\ &\quad + 0.000003\ \text{Raster angle (°)} * \text{Raster angle (°)} \\ &\quad + 0.0016\ \text{Infill density (\%)} * \text{Infill density (\%)} \\ &\quad - 0.001165\ \text{Layer height (mm)} * \text{Raster angle (°)} \\ &\quad + 0.1142\ \text{Layer height (mm)} * \text{Infill density (\%)} \\ &\quad - 0.000439\ \text{Raster angle (°)} * \text{Infill density (\%)}\end{aligned} \tag{3}$$

Response optimizer was used to optimize the predicted fracture strain value within the range inserted printing parameter combination. From this analysis, the maximum fracture strain was found to be 0.0796 mm/mm at a printing

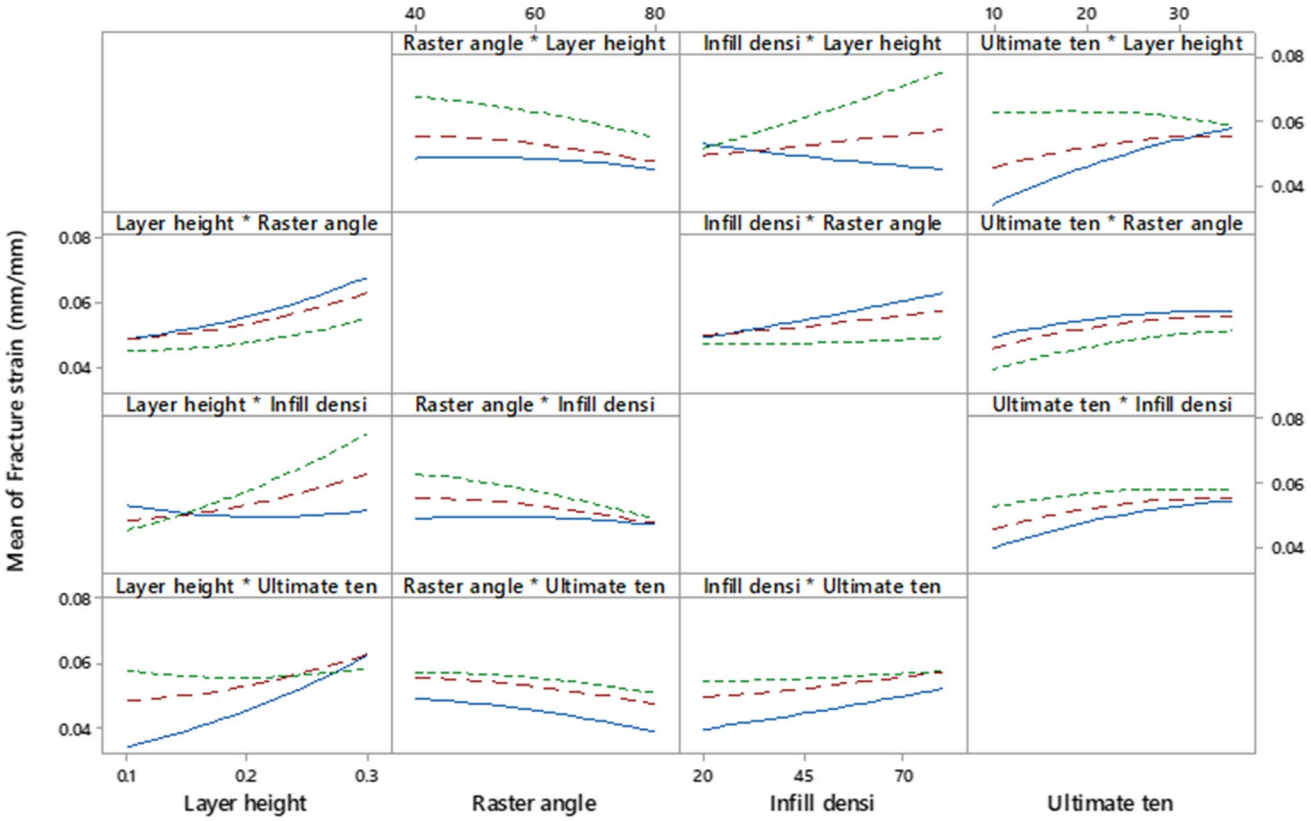

Fig. 14 2-way Interaction of fracture strain

combination of 0.3 mm layer height, 40° raster angle, and 80% infill density.

7 Yield Strength

Table 7 shows that the *p*-value of layer height, raster angle, and infill percentage is more than the alpha value of 0.05, indicating all the parameters are insignificant. This is due to yield strength is affected by other parameters.

$$\begin{aligned}\text{Yield strength (MPa)} = {} & 32.8 + 62.3\ \text{Layer height (mm)} \\ & - 1.188\ \text{Raster angle (°)} + 56.1\ \text{Infill density (\%)} \\ & + 34\ \text{Layer height (mm)} * \text{Layer height (mm)} + 0.01010\ \text{Raster angle (°)} * \text{Raster angle (°)} \\ & - 31.6\ \text{Infill density (\%)} * \text{Infill density (\%)} \\ & - 0.299\ \text{Layer height (mm)} * \text{Raster angle (°)} \\ & - 91.8\ \text{Layer height (mm)} * \text{Infill density (\%)} \\ & - 0.045\ \text{Raster angle (°)} * \text{Infill density (\%)}\end{aligned} \tag{4}$$

8 Comparison of the Experimental and Predicted Mechanical Response

The comparative results of experimental and predicted responses of tensile properties are summarized in Table 8. Table 8 shows that the average error between the experimental value and the predicted value is minimal, ranging from 0.041 to 0.1135%. Hence, all the mathematical models can be highly accounted for reproducing similar tensile properties with minimum deviation.

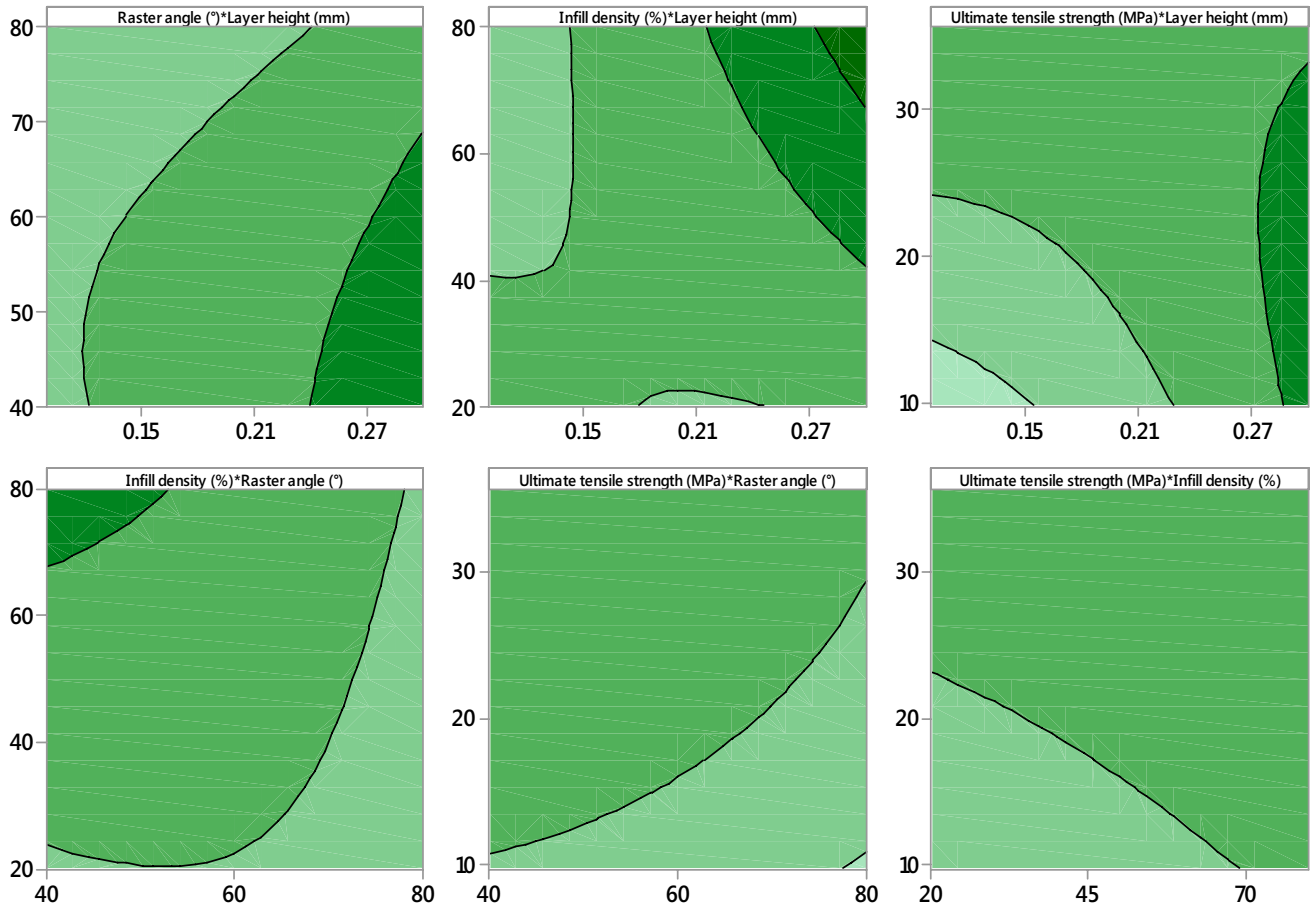

Fig. 15 The contour plot of fracture strain

Table 7 ANOVA table for yield strength

Source	DF	Adj SS	Adj MS	*F*-Value	*p*-Value
Model	9	313.975	34.8862	3.46	0.013
Linear	3	70.792	23.5975	2.34	0.109
Layer height (mm)	1	26.415	26.4149	2.62	0.124
Raster angle (°)	1	25.042	25.0423	2.49	0.133
Infill density (%)	1	19.335	19.3352	1.92	0.184
Square	3	147.017	49.0058	4.86	0.013
Layer height (mm) * Layer height (mm)	1	0.705	0.7053	0.07	0.795
Raster angle (°) * Raster angle (°)	1	97.874	97.8739	9.71	0.006
Infill density (%) * Infill density (%)	1	48.438	48.4382	4.81	0.043
2-Way interaction	3	96.166	32.0552	3.18	0.051
Layer height (mm) * Raster angle (°)	1	4.298	4.2985	0.43	0.522
Layer height (mm) * Infill density (%)	1	90.998	90.9983	9.03	0.008
Raster angle (°) * Infill density (%)	1	0.869	0.8689	0.09	0.773
Error	17	171.277	10.0751		
Total	26	485.253			

Table 8 Overall comparison between the experimental and predicted response

No.	Parameters			Ultimate tensile strength (MPa)		Fracture strain (mm/mm)		Elastic Modulus (MPa)		Yield strength (MPa)	
	Layer height (mm)	Raster angle (°)	Infill density (%)	Actual	Predicted	Actual	Predicted	Actual	Predicted	Actual	Predicted
1	0.1	40	20	19.13284	15.518	0.04696	0.0427	471.36800	475.28	14.80733	14.5740
2	0.2	40	20	20.62756	20.576	0.04749	0.0479	592.43518	585.92	20.24389	18.7920
3	0.3	40	20	25.47271	25.434	0.05649	0.0553	664.50571	682.16	23.25575	23.6900
4	0.1	40	50	20.01269	20.942	0.04944	0.0480	617.45320	587.99	18.20973	21.4740
5	0.2	40	50	22.07215	23.774	0.05638	0.0566	681.82740	655.97	25.96373	22.9380
6	0.3	40	50	27.60767	26.406	0.06299	0.0675	687.48530	709.55	25.41023	25.0820
7	0.1	40	80	32.93754	29.354	0.05201	0.0537	807.48931	802.4	26.08234	22.6860
8	0.2	40	80	25.98610	29.96	0.06221	0.0657	811.80500	827.72	17.15938	21.3960
9	0.3	40	80	28.45150	30.366	0.08012	0.0800	828.06000	838.64	20.19923	20.7860
10	0.1	60	20	9.737220	13.702	0.03667	0.0433	277.74950	327.06	9.02682	10.2360
11	0.2	60	20	14.62170	18.236	0.04234	0.0461	411.37350	441.24	11.71857	13.8560
12	0.3	60	20	21.89921	22.57	0.04725	0.0513	569.91250	541.02	17.94593	18.1560
13	0.1	60	50	18.62290	20.308	0.04301	0.0460	502.59040	478.83	15.39083	16.8660
14	0.2	60	50	23.50263	22.616	0.05779	0.0523	548.66390	550.35	17.06961	17.7320
15	0.3	60	50	29.91145	24.724	0.05955	0.0608	666.89560	607.47	22.90661	19.2780
16	0.1	60	80	27.74211	29.902	0.04633	0.0490	688.12960	732.3	22.57436	17.8080
17	0.2	60	80	34.44592	29.984	0.05962	0.0587	765.41520	761.16	12.13855	15.9200
18	0.3	60	80	31.31328	29.866	0.07797	0.0707	779.47400	775.62	15.59510	14.7120
19	0.1	80	20	17.45173	15.526	0.04544	0.0463	441.46120	402.92	15.45240	13.9780
20	0.2	80	20	24.13670	19.536	0.04641	0.0468	545.66240	520.64	21.76234	17.0000
21	0.3	80	20	21.26233	23.346	0.05212	0.0496	620.03750	623.96	16.53470	20.7020
22	0.1	80	50	21.33669	23.314	0.04587	0.0464	563.48140	593.75	17.40802	20.3380
23	0.2	80	50	26.51747	25.098	0.04700	0.0503	637.79120	668.81	22.64616	20.6060
24	0.3	80	50	24.16019	26.682	0.05428	0.0565	671.07330	729.47	20.64242	21.5540
25	0.1	80	80	35.61776	34.09	0.04823	0.0467	912.16466	886.28	19.77362	21.0100
26	0.2	80	80	31.40398	33.648	0.05116	0.0541	930.57890	918.68	17.84010	18.5240
27	0.3	80	80	32.13470	33.006	0.05637	0.0637	952.17360	936.68	18.04070	16.7180
Average error (%)				0.101		0.053		0.041		0.1135	

Table 9 Comparison of the overall optimized mechanical response

	Layer height (mm)	Raster angle (°)	Infill density (%)	Ultimate tensile strength (MPa)	Elastic modulus (MPa)	Fracture strain (mm/mm)	Yield strength (MPa)
Experimental	0.3	40	80	28.452	828.060	0.08012	20.1992
Predicted	0.3	40	80	30.356	838.367	0.07960	20.7879

9 Multiple Response Prediction

In the previous subtopic, all four responses were optimized individually to determine the maximum achievable value. However, using multiple response prediction, the optimized overall response in conjunction with one printing parameter combination can be determined. This analysis found that the best parameter combination for optimum tensile properties was 0.3-mm layer thickness, 40° raster angle, and 80% infill density. The values are listed in Table 9.

10 Conclusion

In this research work, 81 specimens with 27 different printing parameter combinations were successfully printed using the low-cost FDM 3D printer. Tensile testing was performed to evaluate each specimen's tensile properties and investigate the effect of printing parameters on the tensile behavior. The highest UTS, strain, elastic modulus, yield strength, and toughness obtained in the present study is 35.61776 MPa, 0.08012 mm/mm, 952.1736 MPa, 26.08234 MPa, and 1.82228 J/m^3, respectively. From the observation of the trends, it can be concluded that ultimate tensile strength is predominantly affected by the infill percentage and very least affected by raster angle and layer thickness. On the other hand, it is found that fracture strain, elastic modulus, and toughness are more influenced by the infill percentage and layer thickness. The best-suited combined parameter for optimum tensile properties from the experimental analysis is 0.3 mm layer height, 40° raster angle, and 80% infill density. The resulting properties are 28.45150 MPa for UTS, 0.08012 mm/mm for fracture strain, 828.0600 MPa for elastic modulus, 20.19923 MPa for yield strength and 1.72182 J/m^3 for toughness. The RSM analysis further affirms that's infill density is the primary factor influencing the tensile behavior. The R^2 value for all the examinations obtained to be more than 80%, suggesting reliable experimental data. A second-order mathematical model is developed for each tensile property for estimation of the properties. Validation of the model reveals very minimal error ranging from 0.041 to 0.1135%. Thus, the models can be highly accounted for reproducing similar tensile properties with minimum deviation. Finally, the multiple response prediction reveals the possible parameter combination for the best tensile properties. The best parameter combination for optimum tensile properties was 0.3 mm layer thickness, 40° raster angle, and 80% infill density.

Acknowledgements The authors are grateful to Universiti Malaysia Pahang (www.ump.edu.my) for the financial support provided under the Grants RDU192216, RDU190352, and RDU192403.

References

1. Lanzotti, A., et al.: The impact of process parameters on mechanical properties of parts fabricated in PLA with an open-source 3-D printer. Rapid Prototyp. J. **21**(5), 604–617 (2015)
2. Mpofu, T.P., Mawere, C., Mukosera, M.: The impact and application of 3D printing technology (2014)
3. Chen, L., et al.: The research status and development trend of additive manufacturing technology. Int. J. Adv. Manuf. Technol. **89**(9–12), 3651–3660 (2017)
4. Afrose, M.F., et al.: Effects of build orientations on tensile properties of PLA material processed by FDM. In: Advanced Materials Research (2014). Trans Tech Publ
5. Tian, X., et al.: Interface and performance of 3D printed continuous carbon fiber reinforced PLA composites. Compos. A Appl. Sci. Manuf. **88**, 198–205 (2016)
6. Ahmed, A., Susmel, L.: Additively Manufactured PLA under static loading: strength/cracking vs behaviour deposition angle. Procedia Struct. Integr. 3, 498–507 (2017)
7. Torres, J., et al.: Mechanical property optimization of FDM PLA in shear with multiple objectives. Jom **67**(5), 1183–1193 (2015)
8. Afrose, M.F., et al.: Effects of part build orientations on fatigue behaviour of FDM-processed PLA material. Prog. Addit. Manuf. **1**(1–2), 21–28 (2016)
9. Sood, A.K.; Ohdar, R.K.; Mahapatra, S.S.: Parametric appraisal of mechanical property of fused deposition modelling processed parts. Mater. Des. **31**(1), 287–295 (2010)
10. Forster, A.M.: Materials testing standards for additive manufacturing of polymer materials. ST, Department of Commerce, NI (2015)
11. Zein, I., et al.: Fused deposition modeling of novel scaffold architectures for tissue engineering applications. Biomaterials **23**(4), 1169–1185 (2002)
12. Domingo-Espin, M., et al.: Mechanical property characterization and simulation of fused deposition modeling Polycarbonate parts. Mater. Des. **83**, 670–677 (2015)
13. Wu, W., et al.: Influence of layer thickness and raster angle on the mechanical properties of 3D-printed PEEK and a comparative mechanical study between PEEK and ABS. Materials **8**(9), 5834–5846 (2015)
14. Ning, F., et al.: Additive manufacturing of carbon fiber-reinforced plastic composites using fused deposition modeling: Effects of process parameters on tensile properties. J. Compos. Mater. **51**(4), 451–462 (2017)
15. Bellini, A.; Güçeri, S.: Mechanical characterization of parts fabricated using fused deposition modeling. Rapid Prototyp. J. **9**(4), 252–264 (2003)
16. Ahn, S.-H., et al.: Anisotropic material properties of fused deposition modeling ABS. Rapid Prototyp. J. **8**(4), 248–257 (2002)
17. Bagsik, A., Schöppner, V., Klemp, E.: FDM part quality manufactured with Ultem* 9085. In: 14th International Scientific Conference on Polymeric Materials (2010)
18. Li, H., et al.: The effect of process parameters in fused deposition modelling on bonding degree and mechanical properties. Rapid Prototyp. J. **24**(1), 80–92 (2018)
19. Es-Said, O., et al.: Effect of layer orientation on mechanical properties of rapid prototyped samples. Mater. Manuf. Processes **15**(1), 107–122 (2000)
20. Habeeb, H., et al.: Strength and porosity of additively manufactured PLA using a low cost 3D printing. Proc. Mech. Eng. Res. Day **2016**, 69–70 (2016)
21. Zhou, X., Hsieh, S.-J., Ting, C.-C.: Modelling and estimation of tensile behaviour of polylactic acid parts manufactured by fused deposition modelling using finite element analysis and knowledge-based library. Virtual and Physical Prototyping, pp. 1–14 (2018)
22. Pires, F.Q., et al.: Predictive models of FDM 3D printing using experimental design based on pharmaceutical requirements for tablet production. Int. J. Pharm. **588**, 119728 (2020)
23. Anitha, R.; Arunachalam, S.; Radhakrishnan, P.: Critical parameters influencing the quality of prototypes in fused deposition modelling. J. Mater. Process. Technol. **118**(1–3), 385–388 (2001)
24. Ang, K.C., et al.: Investigation of the mechanical properties and porosity relationships in fused deposition modelling-fabricated porous structures. Rapid Prototyp. J. (2006)
25. Mohamed, O.A.; Masood, S.H.; Bhowmik, J.L.: Optimization of fused deposition modeling process parameters: a review of current research and future prospects. Adv. Manuf. **3**(1), 42–53 (2015)

26. Gross, B.C., et al.: Evaluation of 3D Printing and Its Potential Impact on Biotechnology and the Chemical Sciences. ACS Publications (2014)
27. Huang, S.H., et al.: Additive manufacturing and its societal impact: a literature review. Int. J. Adv. Manuf. Technol. **67**(5–8), 1191–1203 (2013)
28. Onwubolu, G.C., Rayegani, F.: Characterization and optimization of mechanical properties of ABS parts manufactured by the fused deposition modelling process. International Journal of Manufacturing Engineering (2014)
29. Norma, A.: Standard Test Method for Tensile Properties of Plastics. Annu. B. ASTM Stand, pp. 1–15 (2014)
30. Panda, S.K., et al.: Optimization of fused deposition modelling (FDM) process parameters using bacterial foraging technique. Intell. Inf. Manag. **1**(02), 89 (2009)